PHYSICAL REVIEW B **91**, 104425 (2015)

Spin reorientation transition in dysprosium-samarium orthoferrite single crystals

Weiyao Zhao, Shixun Cao,* Ruoxiang Huang, Yiming Cao, Kai Xu, Baojuan Kang, Jincang Zhang, and Wei Ren†
Department of Physics, and International Center of Quantum and Molecular Structures, Shanghai University, Shanghai 200444, China

(Received 13 July 2014; revised manuscript received 24 February 2015; published 26 March 2015)

We report the control of spin reorientation (SR) transition in perovskite $Dy_{1-x}Sm_xFeO_3$, a whole family of single crystals grown by an optical floating zone method from $x = 0$ to 1 with an interval of 0.1. Powder x-ray diffractions and Rietveld refinements indicate that lattice parameters a and c increase linearly with Sm doping concentration, whereas b keeps a constant. Temperature dependence of the magnetizations under zero-field-cooling (ZFC) and field-cooling (FC) processes are studied in detail. We have found a remarkable linear change of SR transition temperature in Sm-rich samples for $x > 0.2$, which covers an extremely wide temperature range including *room* temperature. The a-axis magnetization curves under the FC during cooling (FCC) process bifurcate from and then jump back to that of the ZFC and FC warming process in single crystals when $x =$ 0.5−0.9, suggesting complicated $4f-3d$ electron interactions among Dy^{3+}-Sm^{3+}, Dy^{3+}-Fe^{3+}, and Sm^{3+}-Fe^{3+} sublattices of diverse magnetic configurations. The magnetic properties from the doping effect on SR transition temperature in these single crystals might be useful in the material physics and device design applications.

DOI: 10.1103/PhysRevB.91.104425 PACS number(s): 75.60.Jk, 75.50.Ee, 75.50.Ss, 75.85.+t

I. INTRODUCTION

Rare earth orthoferrites ($RFeO_3$) possessing two magnetic ions, rare earth R^{3+} and iron Fe^{3+} ions, crystallize in an orthorhombic lattice with *Pbnm* space group which is a distorted perovskite structure [1,2]. As a functional material family, $RFeO_3$ is of fundamental scientific interest and technological importance for potential applications such as ultrafast optomagnetic recording [3–6], laser-induced thermal spin reorientation [7,8], precession excitation induced by terahertz pulses [9,10], inertia-driven spin switching [11], and magnetism-induced ferroelectric multiferroics [12–15]. $RFeO_3$ is drawing increasing attention because of emergent technologies which need compounds [5] that exhibit striking physical properties in areas such as magnetic anisotropy and electric field control of magnetism. Recently, an improper ferroelectricity and spontaneous magnetization reversal in $SmFeO_3$ have been reported [16], and quickly stimulated further investigations of this particular oxide [5,17,18]. And for $DyFeO_3$, versatile and gigantic magnetoelectric effects have been experimentally found in a single crystal with a magnetic-field-induced ferroelectric state [15], followed by an *ab initio* study revealing the role of $4f$ electrons in stabilizing the multiferroic state of $DyFeO_3$ [19]. In $RFeO_3$ structures, two metallic ions provide three magnetic interactions, namely Fe^{3+}-Fe^{3+}, Fe^{3+}-R^{3+}, and R^{3+}-R^{3+} couplings. The strongest magnetic interaction of those three is a G-type antiferromagnetic Fe^{3+}-Fe^{3+} interaction which causes the iron ions to orient opposite to all nearest neighbors in three dimensions below the first Néel temperature (T_{N1}) at 650–700 K. However, the iron spin directions are not completely collinear but are slightly canted with respect to one another. There are two canting types, a so-called *hidden canting* causing a C-type or A-type antiferromagnet, and the other *overt canting* causing a net moment (F) [2]. Due to symmetry considerations and the antiferromagnetic *nature* of the coupling between the ions, there are three magnetic configurations allowed for the Fe^{3+} sublattices: the Γ_1, Γ_2, and Γ_4 configurations with different antiferromagnetic directions. In the Γ_1 configuration there is no net magnetization F along any direction and the major G-type antiferromagnetic vector points along the b axis (A_x, G_y, C_z). The Γ_2 configuration is characterized by the net moment F pointing along the a axis and the major G-type antiferromagnetism lining along the c axis (F_x, C_y, G_z). The Γ_2 configuration can be rotated such that the net moment aligns along the c axis and major G-type antiferromagnetism lines along the a axis, then we obtain the Γ_4 configuration (G_x, A_y, F_z). Most $RFeO_3$ members have quite different temperature dependent spin configurations. The Γ_4 configuration can be found in all $RFeO_3$ in high-temperature regions while any of three mentioned configurations might be found at lower temperature. If the high-temperature configuration is different from that of low temperature, a transition called spin reorientation (SR) will take place in a certain temperature range (T_{SR}). When SR happens, the direction of easy axis of magnetization of Fe^{3+} sublattice changes from one crystallographic axis to another upon varying the temperature. Furthermore, rare earth F moments may polarize parallel or antiparallel to the net iron sublattice moment. For the orthoferrites which undergo SR transition, the relative orientation of the iron and rare-earth net moments may be the same (keeping either parallel or antiparallel) above and below the transition (e.g., $ErFeO_3$), or may change relative orientation (between parallel and antiparallel) by the transition (e.g., $YbFeO_3$, $TmFeO_3$) [1]. Finally, at low enough temperatures (on the order of 10 K or less), R^{3+}-R^{3+} interaction may cause an ordering of rare-earth ions at a second Néel temperature (T_{N2}) [1].

The origin of SR is the competition between different spin configurations which possess different free energy. The main exchange energy of $RFeO_3$ structure is provided by iron sublattice exchange interaction which is two orders larger than the others. The energy of R^{3+}-Fe^{3+} ($4f-3d$ electrons) interaction which plays crucial roles in SR is rather small compared with that of Fe^{3+}-Fe^{3+} interaction, but larger than or of the same order of the *anisotropy* energy of R^{3+}-R^{3+} interaction. As

---

*sxcao@shu.edu.cn
†renwei@shu.edu.cn

temperature decreases, all of the magnetic interactions will be enhanced with different degrees, and SR occurs when the Fe^{3+}-R^{3+} interaction increases to a comparable magnitude with the anisotropy energy of Fe^{3+}-Fe^{3+} interaction. We may find two types of SR processes with respect to the different spin configurations of RFeO$_3$. One is that the net moment begins to rotate at temperature T_1, and ceases rotating with the rotation angle of 90 deg at temperature T_2 (NdFeO$_3$, SmFeO$_3$, TbFeO$_3$, HoFeO$_3$, ErFeO$_3$, TmFeO$_3$, and YbFeO$_3$, from Γ_2 to Γ_4 [1,20–24]), while the other transition takes place abruptly at a phase transition temperature T_r (DyFeO$_3$ [25–27] and CeFeO$_3$ [28], from Γ_1 to Γ_4). It is interesting to determine SR in orthoferrites which possess these two distinct SRs, as we introduce both Sm (Γ_2 to Γ_4) and Dy (Γ_1 to Γ_4) to RFeO$_3$ in this study. Another strong motivation for us is to produce SR effect at *room* temperature by combining the highest T_{SR} of all RFeO$_3$ (SmFeO$_3$) and a low temperature T_r (DyFeO$_3$). In what follows we focus on the change of magnetic configurations in dysprosium-samarium orthoferrites, the interaction between Dy and Sm moments, and $4f-3d$ electrons interaction which influence the doping concentration effect on the SR transition temperature.

II. EXPERIMENTS

A whole family of single crystals $Dy_{1-x}Sm_xFeO_3$ (DSFO) with 11 different x values were successfully grown by an optical-floating-zone method (Crystal System Inc., type FZ-T-10000-H-VI-P-SH). The compounds of feed and seed rods were prepared by the solid state reaction of the ternary raw materials Sm_2O_3(99.9%), Dy_2O_3(99.9%), and Fe_2O_3(99.99%), with the proper cation stoichiometry which was calculated by the target compound. The temperature of the molten zone was controlled by adjusting the power of lamps. During the growth process, the molten zone moved upwards at a rate of 1–3.5 mm/h, with the seed rod (lower shaft) and the feed rod (upper shaft) counter rotating at 30 rpm in flow air [29–33]. All of their crystallographic orientations were determined by an x-ray Laue photograph (Try-SE. Co, Ltd.). X-ray diffraction (XRD, Rigaku 18 kW D/MAX 2550) with Cu$-K_\alpha$ radiation at $\lambda = 1.5406$ Å was used to determine the crystal structures using the powders made by grinding part of the single crystal samples. Measurements of magnetization as functions of temperature and magnetic field were performed using the Physics Property Measurement System (Quantum Design, PPMS-9). Zero-field-cooling (ZFC) and field-cooling (FC) processes were used to acquire the temperature dependence of the magnetization. The measurements of ZFC and FCW curves were performed during warming process while the FCC curve was performed during the cooling process.

III. RESULTS AND DISCUSSION

Figure 1(a) shows the experimental powder XRD patterns of the DSFO family with a content change interval $\Delta x = 0.1$ at room temperature. The XRD powders were made by grinding part of the single crystal samples. To illustrate clearly the differences in the diffraction signals, a zoom-in between 31 and 35 deg is shown in Fig. 1(b) where significant shift of the main peak (112) is observed. It is also clearly shown that the peak (020) near 32 deg does not shift, which is consistent with the unchanged crystal structure parameter b [see also Fig. 1(c)]. Rietveld refinement [34] of crystal structures based on an orthorhombic structure with *Pbnm* space group from the Fullprof program [35] shows that no impurity phase was detected in all samples. Structure parameters a, b, and c of the samples are calculated and summarized in Fig. 1(c) from the Rietveld refinement. As Sm content x increases, the lattice parameter b remains unchanged at about 5.60 Å, but both parameters a and c increase linearly from 5.30 to 5.40 Å for a and 7.62 to 7.70 Å for c, respectively. Such an increase is comprehensible since the Sm ion is larger than the Dy ion and thus induces larger lattice parameters of the perovskite structure. Similar structural changes induced by the rare earth radii have been theoretically investigated in RCrO$_3$ and RFeO$_3$ compounds [36,37]. Importantly, it provides us the controllability of SR temperature through Sm and Dy concentration tuning in the single crystal samples as discussed below.

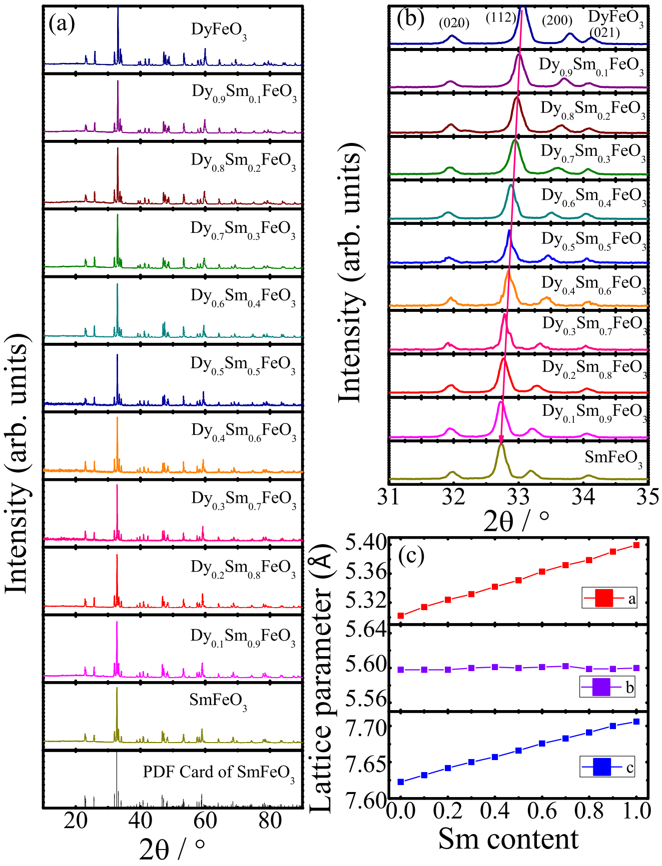

FIG. 1. (Color online) (a) X-ray diffraction patterns of the DSFO single crystal family, the standard diffraction of SmFeO$_3$ (PDF#74-1474) is plotted in the bottom panel. (b) Zoom-in of (a) for 2θ between 31 and 35 deg, the line is a guide for the eyes as Sm doping is increasing. (c) Lattice parameters of the DSFO family calculated by the Rietveld refinement using the XRD data with different Sm doping concentrations; the parameters a, b, and c can be fitted very well by three straight lines.

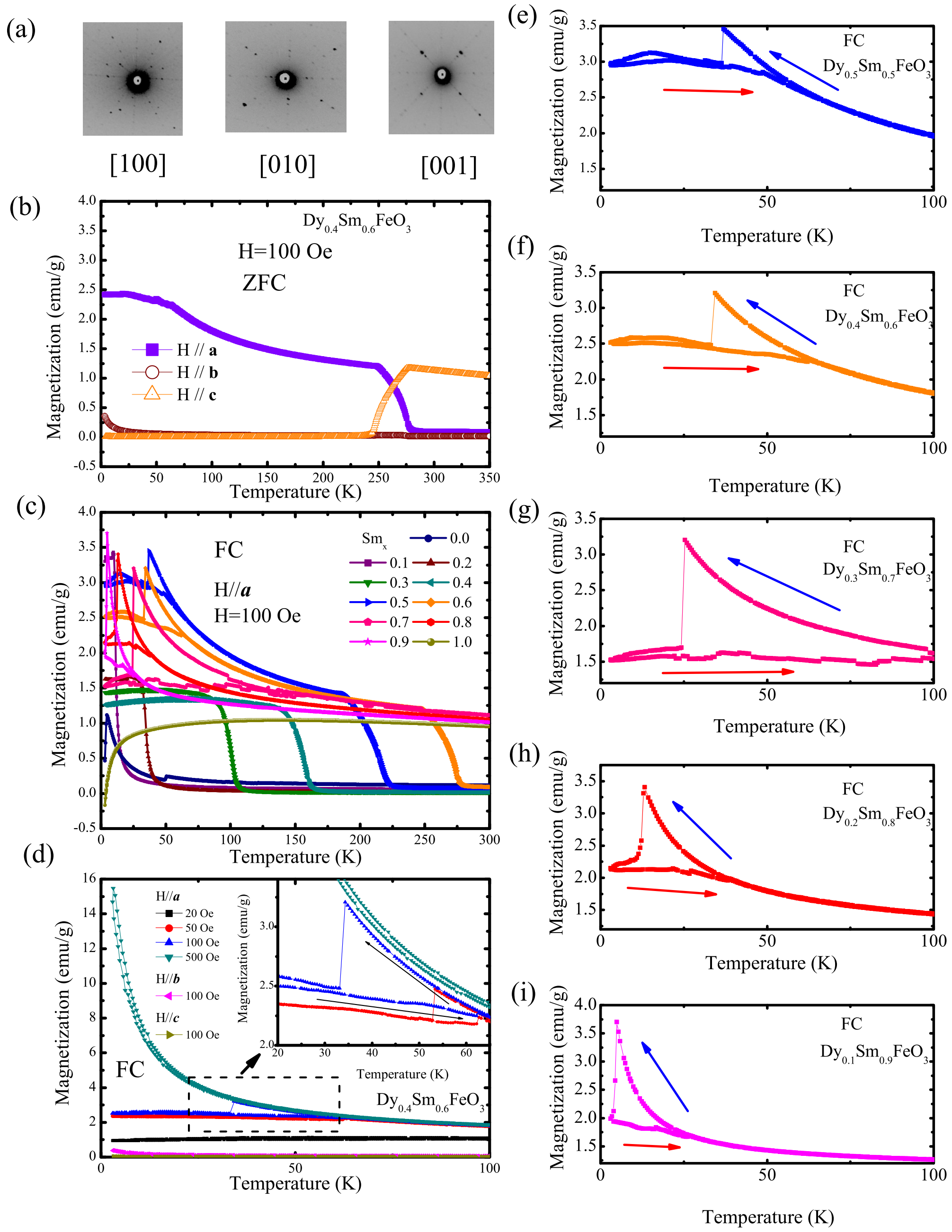

FIG. 2. (Color online) (a) X-ray Laue photographs for the a, b, and c axis are taken at room temperature for the crystal $Dy_{0.4}Sm_{0.6}FeO_3$. (b) ZFC magnetizations as a function of temperature for $Dy_{0.4}Sm_{0.6}FeO_3$ under an applied magnetic field of 100 Oe in the temperature range from 3 to 350 K. (c) FC magnetizations along the a axis as a function of temperature for $Dy_{1-x}Sm_xFeO_3$ under an applied magnetic field of 100 Oe in the temperature range from 3 to 300 K. (d) The FCC and FCW curves of $Dy_{0.4}Sm_{0.6}FeO_3$ crystal, with different applied field. Zoom-in FC curves which possess jumping behavior are shown in (e)–(i).

Figure 2(a) display the x-ray Laue photographs for the a, b, and c axes which were taken at room temperature for the crystal $Dy_{0.4}Sm_{0.6}FeO_3$ as a representative. Figure 2(b) shows the magnetizations vs temperature ($M-T$ along a, b, and c axes) of the $Dy_{0.4}Sm_{0.6}FeO_3$ single crystal under the ZFC process as a representative sample, which exhibits SR transition near room temperature. The $M-T$ curve of a axis shows a plateau below 34 K and decreases monotonously during further warming. This behavior is quite different from the $M-T$ of $SmFeO_3$ in which the Sm moment aligns antiparallel to the net Fe moment [17,24,38]. It is clearly shown that under low temperature the net Fe moment orientates along the a axis, which is the feature of Γ_2 spin configuration. An abrupt change at 242 K indicates the beginning of SR, after which further warming results in the easy axis rotation and the a-axis magnetization rapidly declines while the c-axis magnetization increases to a comparable magnitude. Another critical point at 273 K indicates the end of SR, beyond which it is seen that the c-axis magnetization gradually decreases until T_{N1} in a further warming process. The b-axis magnetization shows an upturn below 50 K associated with the ordering of paramagnetic rare earth ions, below which the configuration is $(F_x, C_y, G_z;\ F_x^R, C_y^R)$.

Now we discuss the FCC magnetizations vs temperature as shown in Figs. 2(c) and 2(d). The magnetizations along the b and c axes show no difference during ZFC, FCC, and FCW processes. But as shown in Figs. 2(e)–2(i), the a-axis FCC magnetization curves of $x = 0.5$–0.9 samples is separated from that of the warming measurement (ZFC and FCW) curves. Upon cooling, the FCC curve increases much more significantly than the warming curves until a proper temperature when FCC jumps down to the level of warming curves. It is reasonable to think that a parallel state of Sm moment under FCC is metastable since the Sm moment tends to be antiparallel coupled with the net moment of Fe sublattice [16,17]. Rare earth moments increase as the temperature decreases, which leads to a larger magnetic potential energy. When the temperature is decreased separation temperature, the potential energy of the metastable state is accumulated so large that Sm moments switch to the opposite direction, and thus the total magnetization of the FCC curve drops back to the value of warming curves (ZFC and FCW). During the warming processes of ZFC and FCW, however, the stable states will never make the jump to the metastable one. Furthermore, FCC measurements reveal that the abrupt drop of magnetization eventually disappears when we apply a higher magnetic field of 500 Oe. The magnetization keeps increasing smoothly as the temperature decreases under strong fields seen in Fig. 2(d). As shown in Figs. 2(c) and 2(e)–2(i), all of the FCC curves jumping peaks shift to lower temperature as the Sm concentration increases. This trend of jumping temperature shifts is opposite to that of the SR temperature which is increasing with the Sm content. Note that Dy and Sm total moments are parallel and antiparallel to Fe total moments, respectively. This suggests that Sm^{3+}-Fe^{3+} interaction is suppressed by the presence of Dy^{3+}, whereas both Fe^{3+} and Dy^{3+} total moments are parallel to the external magnetic field during the FCC. Moreover, we have some additional measurements to prove the metastable state in sample $x = 0.6$ shown in Figure 2(d). The FCC and FCW curves were obtained at different applied fields. Jumping peaks appear at 34 K (for 100 Oe) and 52 K (for 50 Oe), but there is no jumping in the 20 Oe curve and the 500 Oe curve. The metastable states are induced by applied field, if the field is too small to induce or too large to keep the stability, jumping behaviors will vanish.

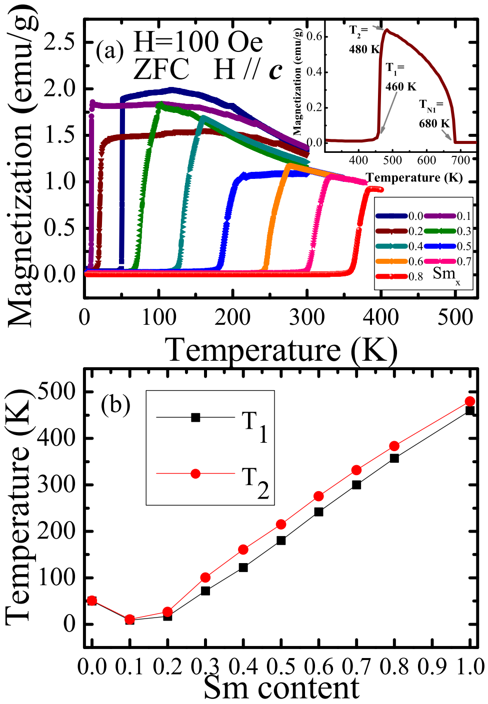

FIG. 3. (Color online) (a) ZFC magnetizations of the DSFO single crystal family as a function of temperature under an applied magnetic field along the c axis, 100 Oe in the temperature range from 3 to 400 K, the inset shows c-axis magnetization of $\mathrm{SmFeO_3}$ at 300−750 K. (b) SR temperatures for the DSFO single crystal family versus Sm concentration, T_1 is the temperature when SR begins from low-temperature configuration, while T_2 is the ending temperature of SR transition.

Figure 3(a) shows c-axis ZFC magnetization measurements of the DSFO crystal family. The SR transition is also clearly shown in each curve, and for $x = 0, 0.1, 0.2$ it is observed that the abrupt changes in SR transition take place in a very narrow temperature range. The other curves ($x > 0.2$) show inflection in the transition temperature regions which correspond to a Landau second-order continuous phase transition, and have the same high-temperature magnetization behavior. It is also notable that above T_2 SR temperatures, the total ZFC magnetizations along the c axis are reduced significantly with an increase of Sm content. The inset displays c-axis magnetization of pure $\mathrm{SmFeO_3}$ in the temperature range of 300–700 K measured by a high temperature vibrating sample magnetometer (VSM), showing typical magnetic property for Sm-rich ($x > 0.2$) single crystal samples. All our measured SR transition temperatures are summarized in Fig. 3(b), by showing the start and ending SR temperatures for each sample. Sm-rich or Dy-rich ($x < 0.2$) samples belong to different SR types resembling their parent compounds, and the majority of DSFO samples follow a linear relationship between the SR temperatures and Sm contents.

The above results provide us useful knowledge for practical control of the SR transition temperature and the SR type through proper doping concentration. A series of interactions from R^{3+} and Fe^{3+} ions have distinguished phenomena during the SR process, and for this reason a precise control of SR becomes important. The results in Fig. 3(b) allows us to select samples whose SR temperature appear in 50−480 K (Γ_2 to Γ_4) with a second-order transition or a sharp SR transition occurring in 10–50 K (Γ_1 to Γ_4). It is known that $\mathrm{SmFeO_3}$ has a particular R^{3+}-Fe^{3+} interaction and possesses a SR transition temperature as high as 480 K [16,17], which is much higher than any other rare-earth orthoferrites. It is thus reasonable that the Sm^{3+}-Fe^{3+} interaction is strong enough compared with the anisotropy part of the Fe^{3+}-Fe^{3+} interaction in the relatively high-temperature region [24], while the other R^{3+}-Fe^{3+} interaction in rare-earth orthoferrites is much smaller. Dy's appearance in the Sm site of $\mathrm{SmFeO_3}$ will naturally reduce the intensity of the Sm^{3+}-Fe^{3+} interaction and decrease the SR temperature in the doped crystals. Dy:Sm concentration changes the lattice parameters a and c much more significantly than the parameter b, which might be correlated to the linear reduction of the Sm^{3+}-Fe^{3+} interaction. R-site doping affects much less on the Fe^{3+}-Fe^{3+} interaction since this interaction is mainly determined by the parameter b [39]. In Dy-doped $SmFeO_3$, the R^{3+}-Fe^{3+} interaction energy is reduced by Dy concentration almost linearly for the temperature higher than 50 K. The SR transition of $DyFeO_3$ (at about 50 K) [13] hints to a comparable magnitude of Dy^{3+}-Fe^{3+} interaction energy and Fe^{3+}-Fe^{3+} anisotropy interaction energy. Meanwhile, a competing effect of the Sm^{3+}-Fe^{3+} interaction and the Dy^{3+}-Fe^{3+} interaction will take place when the temperature is lower than 50 K. When the Dy concentration is dominantly prevalent, the Sm^{3+}-Fe^{3+} interaction is effectively reduced to a normal R^{3+}-Fe^{3+} interaction magnitude so that it will not provide an SR transition higher than 50 K. As a result, the first-order transition occurs when the Dy^{3+}-Fe^{3+} interaction energy is up to a comparable magnitude to the Fe^{3+}-Fe^{3+} anisotropy interaction energy, and it is the case for $x < 0.2$ in this study.

IV. CONCLUSION

In conclusion, doping controlled spin reorientation effects of the DSFO single crystal family have been investigated systematically. Powder x-ray diffraction and Rietveld refinement study indicate that lattice parameters change linearly with the Sm doping content, which correlates with a remarkable linear change of SR transition temperature of the DSFO family. Tuning the binary rare earth elements and contents thus provides a feasible way to obtain magnetic materials with desired SR transition temperature and SR type, even at room temperature for possible multiferroics and spintronics applications. The a-axis magnetization curves under the FCC process bifurcates from and then jumps back to that of the warming process (ZFC and FCW curves) in single crystals $Dy_{1-x}Sm_xFeO_3$ for $x = 0.5-0.9$ with complicated interactions among Dy^{3+}-Sm^{3+}, Dy^{3+}-Fe^{3+}, and Sm^{3+}-Fe^{3+} sublattices, leading to the unexplored venue of magnetic configurations in the rare earth orthoferrites system.

ACKNOWLEDGMENTS

This work is supported by the National Key Basic Research Program of China (Grant No. 2015CB921600), the National Natural Science Foundation of China (NSFC, No. 51372149, No. 11274221, No. 11274222), Eastern Scholar Program and Shuguang Program (Grant No. 12SG34) from Shanghai Municipal Education Commission, QiMingXing Project (14QA1402000), Shanghai Pujiang Program (13PJD015), and Science and Technology Commission of Shanghai Municipality (13ZR1415200).

---

[1] R. L. White, J. Appl. Phys. **40**, 1061 (1969).

[2] T. Yamaguchi, J. Phys. Chem. Solids **35**, 479 (1974).

[3] K. Vahaplar *et al.*, Phys. Rev. B **85**, 104402 (2012).

[4] J. A. de Jong, A. V. Kimel, R. V. Pisarev, A. Kirilyuk, and T. Rasing, Phys. Rev. B **84**, 104421 (2011).

[5] J. A. de Jong, I. Razdolski, A. M. Kalashnikova, R. V. Pisarev, A. M. Balbashov, A. Kirilyuk, T. Rasing, and A. V. Kimel, Phys. Rev. Lett. **108**, 157601 (2012).

[6] A. V. Kimel, C. D. Stanciu, P. A. Usachev, R. V. Pisarev, V. N. Gridnev, A. Kirilyuk, and T. Rasing, Phys. Rev. B **74**, 060403 (2006).

[7] A. V. Kimel, A. Kirilyuk, A. Tsvetkov, R. V. Pisarev, and T. Rasing, Nature (London) **429**, 850 (2004).

[8] L. Le Guyader, A. Kleibert, F. Nolting, L. Joly, P. M. Derlet, R. V. Pisarev, A. Kirilyuk, T. Rasing, and A. V. Kimel, Phys. Rev. B **87**, 054437 (2013).

[9] J. Jiang, Z. Jin, G. Song, X. Lin, G. Ma, and S. Cao, Appl. Phys. Lett. **103**, 062403 (2013).

[10] K. Yamaguchi, T. Kurihara, Y. Minami, M. Nakajima, and T. Suemoto, Phys. Rev. Lett. **110**, 137204 (2013).

[11] A. V. Kimel, B. A. Ivanov, R. V. Pisarev, P. A. Usachev, A. Kirilyuk, and T. Rasing, Nat. Phys. **5**, 727 (2009).

[12] Y. Tokunaga, N. Furukawa, H. Sakai, Y. Taguchi, T.-h. Arima, and Y. Tokura, Nat. Mater. **8**, 558 (2009).

[13] B. Rajeswaran, D. Sanyal, M. Chakrabarti, Y. Sundarayya, A. Sundaresan, and C. N. R. Rao, Europhys. Lett. **101**, 17001 (2013).

[14] Y. Tokura, S. Seki, and N. Nagaosa, Rep. Prog. Phys. **77**, 076501 (2014).

[15] Y. Tokunaga, S. Iguchi, T. Arima, and Y. Tokura, Phys. Rev. Lett. **101**, 097205 (2008).

[16] J. H. Lee, Y. K. Jeong, J. H. Park, M. A. Oak, H. M. Jang, J. Y. Son, and J. F. Scott, Phys. Rev. Lett. **107**, 117201 (2011).

[17] S. X. Cao, H. Z. Zhao, B. J. Kang, J. C. Zhang, and W. Ren, Sci. Rep. **4**, 5960 (2014).

[18] J. H. Lee, Y. K. Jeong, J. H. Park, M. A. Oak, H. M. Jang, J. Y. Son, and J. F. Scott, Phys. Rev. Lett. **108**, 219702 (2012).

[19] A. Stroppa, M. Marsman, G. Kresse, and S. Picozzi, New J. Phys. **12**, 093026 (2010).

[20] J. Yoon *et al.*, Nat. Mater. **7**, 907 (2008).

[21] R. Huang, S. Cao, W. Ren, S. Zhan, B. Kang, and J. Zhang, Appl. Phys. Lett. **103**, 162412 (2013).

[22] S. Yuan, Y. Wang, M. Shao, F. Chang, B. Kang, Y. Isikawa, and S. Cao, J. Appl. Phys. **109**, 07E141 (2011).

[23] S. J. Yuan, W. Ren, F. Hong, Y. B. Wang, J. C. Zhang, L. Bellaiche, S. X. Cao, and G. Cao, Phys. Rev. B **87**, 184405 (2013).

[24] Y. K. Jeong, J. H. Lee, S. J. Ahn, and H. M. Jang, Solid State Commun. **152**, 1112 (2012).

[25] C. E. Johnson, L. A. Prelorendjo, and M. F. Thomas, J. Magn. Magn. Mater. **15–18**, 557 (1980).

[26] L. A. Prelorendjo, C. E. Johnson, M. F. Thomas, and B. M. Wanklyn, J. Phys. C **13**, 2567 (1980).

[27] A. Jaiswal, R. Das, S. Adyanthaya, and P. Poddar, J. Phys. Chem. C **115**, 2954 (2011).

[28] S. J. Yuan, Y. M. Cao, L. Li, T. F. Qi, S. X. Cao, J. C. Zhang, L. E. DeLong, and G. Cao, J. Appl. Phys. **114**, 113909 (2013).

[29] In fact, controlling the cation stoichiometry in the growth of rare earth orthorferrites by changing the growth rate and the gas flow was investigated in a number of earlier studies [30–33]. The mole ratio of rare earth to iron can be controlled by our growth conditions, and will be reflected by the nonexistence of element

volatilization or cracks in all the single crystals here. Under our optimal growth conditions, the compositional concentrations are the same as the nominal amounts of the raw materials.

[30] Y. Wang, S. Cao, M. Shao, S. Yuan, B. Kang, J. Zhang, A. Wu, and J. Xu, J. Cryst. Growth **318**, 927 (2011).

[31] F. Chang, S. Yuan, Y. Wang, S. Zhan, S. Cao, A. Wu, and J. Xu, J. Cryst. Growth **318**, 932 (2011).

[32] M. Shao, S. Cao, Y. Wang, S. Yuan, B. Kang, J. Zhang, A. Wu, and J. Xu, J. Cryst. Growth **318**, 947 (2011).

[33] X. Wang, S. Cao, Y. Wang, S. Yuan, B. Kang, A. Wu, and J. Zhang, J. Cryst. Growth **362**, 216 (2013).

[34] H. M. Rietveld, Acta Crystallogr. **22**, 151 (1967).

[35] J. Rodríguez-Carvajal, Physica B **192**, 55 (1993).

[36] H. J. Zhao, W. Ren, X. M. Chen, and L. Bellaiche, J. Phys.: Condens. Matter **25**, 385604 (2013).

[37] H. J. Zhao, W. Ren, Y. R. Yang, X. M. Chen, and L. Bellaiche, J. Phys.: Condens. Matter **25**, 466002 (2013).

[38] L. G. Marshall, J. G. Cheng, J. S. Zhou, J. B. Goodenough, J. Q. Yan, and D. G. Mandrus, Phys. Rev. B **86**, 064417 (2012).

[39] H. Zhao, S. Cao, R. Huang, W. Ren, S. Yuan, B. Kang, B. Lu, and J. Zhang, J. Appl. Phys. **114**, 113907 (2013).